NANO · MICRO small
www.small-journal.com

A 3-Fluoropyridine Manipulating the Aggregation and Fibril Network of Donor Polymers for Eco-Friendly Solution-Processed Versatile Organic Solar Cells

*Sung Jae Jeon, Nam Gyu Yang, Ji Youn Kim, Ye Chan Kim, Hyoung Seok Lee, and Doo Kyung Moon**

The development of eco-friendly solvent-processed organic solar cells (OSCs) suitable for industrial-scale production should be now considered the imperative research. Herein, asymmetric 3-fluoropyridine (FPy) unit is used to control the aggregation and fibril network of polymer blends. Notably, terpolymer PM6(FPy = 0.2) incorporating 20% FPy in a well-known donor polymer poly[(2,6-(4,8-bis(5-(2-ethylhexyl-3-fluoro)thiophen-2-yl)-benzo[1,2-b:4,5-b']dithiophene))-alt-(5,5-(1',3'-di-2-thienyl-5',7'-bis(2-ethylhexyl)benzo[1',2'-c:4',5'-c']dithiophene-4,8-dione)] (PM6) can reduce the regioregularity of the polymer backbone and endow them with much-enhanced solubility in eco-friendly solvents. Accordingly, the excellent adaptability for fabricating versatile devices based on PM6(FPy = 0.2) by toluene processing is demonstrated. The resulting OSCs exhibit a high power conversion efficiency (PCE) of 16.1% (17.0% by processed with chloroform) and low batch-to-batch variation. Moreover, by controlling the donor-to-acceptor weight ratio at 0.5:1.0 and 0.25:1.0, semi-transparent OSCs (ST-OSCs) yield significant light utilization efficiencies of 3.61% and 3.67%, respectively. For large-area (1.0 cm^2) indoor OSC (I-OSC), a high PCE of 20.6% is achieved with an appropriate energy loss of 0.61 eV under a warm white light-emitting diode (3,000 K) with the illumination of 958 lux. Finally, the long-term stability of the devices is evaluated by investigating their structure–performance–stability relationship. This work provides an effective approach to realizing eco-friendly, efficient, and stable OSCs/ST-OSCs/I-OSCs.

1. Introduction

Organic solar cells (OSCs) based on π-conjugated polymers have enormous potential economic impact in various fields, including buildings, vehicles, sensors, and mini-electronics, owing to their unique features, such as solution-processability, flexibility, lightweight, semi-transparency, and high absorption.[1–5] With the developments in material design and device/interface engineering,[6–8] the power conversion efficiency (PCE) of single-junction OSCs has exceeded 19%,[9–11] which is considerably higher than the commercialization threshold benchmark PCE of 15%.[5] Considering this consistently high PCE, eco-friendly manufacturing has become prominent focus, which is critical to the industrial applications of OSCs.[12] In particular, most efficiency-competitive photoactive materials depend on halogenated solvents, such as chloroform (CF) and chlorobenzene (CB), which are difficult to produce on a large scale, and are detrimental to human health and ecosystems.[9–11,13–16] Therefore, it should be desirable to focus on developing solar cells with non-toxic process considering the eco-friendly fabrication.

Efficient donor polymers adopt regioregular donor (D)–π-acceptor (A)–π structures, inducing high crystallinity to achieve high photovoltaic performance.[7] However, these polymers paradoxically exhibit poor solubility in eco-friendly solvents, such as toluene (TL) and *o*-xylene (XY): although non-halogenated solvents are not perfect green, such solvents enable a safer and environmentally friendlier fabrication process compared to halogenated solvents. To address this issue, several promising terpolymer design strategies have been developed using a third component.[12,17–20] Such terpolymer strategies can be highlighted with additional advantages, such as selective absorption and fine-tuning of frontier energy levels. For example, certain D or A units possess chromophores with the absorption of photons in the long-wavelength region, whereas certain units have deep highest occupied molecular orbital (HOMO) levels, resulting in unique copolymers for different applications.[18]

As shown in Chart S1 (Supporting Information), Lu et al. designed three terpolymers (PL1, PL2, and PL3) by employing repeating units of two high-performance polymers, PM6 and

S. J. Jeon, N. G. Yang, J. Y. Kim, Y. C. Kim, H. S. Lee, D. K. Moon
Nano and Information Materials (NIMs) Laboratory
Department of Chemical Engineering
Konkuk University
120, Neungdong-ro, Gwangjin-gu, Seoul 05029, South Korea
E-mail: dkmoon@konkuk.ac.kr

The ORCID identification number(s) for the author(s) of this article can be found under https://doi.org/10.1002/smll.202301803

DOI: 10.1002/smll.202301803

poly[(2,6-(4,8-bis(5-(2-ethylhexyl-3-fluoro)thiophen-2-yl)-benzo-[1,2-b:4,5-b']dithiophene))-alt-5,5'-(5,8-bis(4-(2-butyloctyl)thiophen-2-yl)dithieno[3',2':3,4;2'',3'':5,6]benzo[1,2-c][1,2,5]thiadiazole)] (D18).[21] The terpolymers reduced the regioregularity of the polymer backbones and endowed them with enhanced solubility in eco-friendly solvents, such as XY . Compared to PM6 (15.16%) and D18 (16.18%), the XY -processed PL1-based OSC exhibits the highest PCE of 18.14% with a lower energy loss (E_{loss}) (obtained by: $E_{loss} = E_g - qV_{oc}$, where E_g is the bandgap from the corresponding external quantum efficiency (EQE) curve, and q is the elementary charge). More recently, Lee et al. reported a series of terpolymers by introducing a hydrophilic oligo(ethylene glycol) (OEG) flexible spacer into the PM6 matrix, which is a well-known efficient donor polymer.[22] Compared with PM6, the OEG-incorporated terpolymers reduced the excessive molecular rigidity of the polymer chains, thereby alleviating their aggregation behavior and promoting their intermixing with the acceptors. Among TL-processed OSCs, PM6-OEG5 achieves the highest PCE of 17.74%. Furthermore, the fabricated stretchable OSCs simultaneously exhibits a high PCE of 12.05% and stretchability of 80% of the initial PCE at a strain of 22% because the OEG flexible spacer increased the mechanical robustness and ductility of the devices.

However, few studies have attempted to fabricate efficient semi-transparent OSCs (ST-OSCs) and indoor OSCs (I-OSCs) using an eco-friendly solution.[18,23–27] Moreover, from an industrialization perspective, the realization of eco-friendly solution-processed ST-OSC/I-OSCs is crucial, and the mechanism of their favorable morphologies remains an open question. Therefore, the choice of processing solvents for fabricating device should be carefully considered because it directly affects not only the device performance, but also, potentially, the film morphology related to the stability.[12,28,29] In various eco-friendly processed devices, where the polymer often results in undesirable morphologies, solvent additives are required to improve the control of the film formation kinetics, thereby optimizing the blend morphology and photovoltaic performance.[30] Notably, solvent additives should be non-halogenated because they affect human health and the environment at the same extent as that of host solvents.[12]

In this study, we designed and synthesized three donor polymers based on an asymmetric 3-fluoropyridine (FPy) unit with a non-covalent conformational dual-lock on one side and free torsion on the other side for eco-friendly solution-processable OSCs. Among them, the terpolymer PM6(FPy = 0.2), incorporating 20% FPy into the PM6 backbone, achieved the highest PCE of 16.1% (17.0% by processing with CF) and reproducibility in the TL-processed OSCs blended with a 2,2′-((2Z,2′Z)-((12,13-bis(2-butyloctyl)-3,9-dinonyl-12,13-dihydro-[1,2,5]thiadiazolo[3,4-e]-thieno[2″,3″:4′,5′]thieno[2′,3′:4,5]pyrrolo[3,2-g]thieno[2′,3′:4,5]-thieno[3,2-b]indole-2,10-diyl)bis(methaneylylidene))bis(5,6-dichloro-3-oxo-2,3-dihydro-1H-indene-2,1-diylidene))dimalononitrile (BTP-eC9). Remarkably, this polymer with a unique aggregation behavior could be finely tuned the fibril network morphology of the polymer blend according to the donor weight ratio. Based on this strategy, all OSCs exhibited reasonable PCEs of 10.1%–16.1% by maintaining a high fill factor (FF) of over 72%, despite the decreased proportion of donor polymer from 100% to 20%. In short, the optimized ST-OSCs yield high PCEs of 11.1% and 8.9% with average visible transmittances (AVTs) of 32.6% and 41.1% at donor-to-acceptor weight ratios of 0.5:1.0 and 0.25:1.0, thereby achieving significant light utilization efficiencies (LUEs) of 3.61% and 3.67%, respectively.

In addition, we demonstrated the great potential of PM6(FPy = 0.2) by matching it with a 4T-BA acceptor for efficient large-area I-OSCs. This polymer blend can cover the entire emission spectra (450–730 nm) of indoor artificial light sources with an appropriate E_{loss} of 0.61 eV. As a result, the optimized I-OSC with an effective area of 1.0 cm^2 exhibits a high PCE of 20.6% with an open-circuit voltage (V_{oc}) of 0.94 V under warm white light-emitting diode (LED; 3000 K) illumination of 958 lux. Notably, the I-OSC showed a PCE of 19.1% at 195 lux, despite the lower light intensity. Finally, we evaluated the long-term stability of all devices, according to the shelf protocol of the International Summit on OSC Stability in Dark Testing-1 (ISOS-D-1). All OSCs/ST-OSCs/I-OSCs showed reasonable storage stabilities under the corresponding conditions. Interestingly, the stability of ST-OSCs was further improved by introducing fewer donor polymers in the polymer blend owing to the fibril networks related to a favorable morphology in terms of long-term stability. Overall, the eco-friendly solution-processable PM6(FPy = 0.2) can achieve efficient multifunctional OSC devices with good stability by manipulating the aggregation and fibril network.

2. Results and Discussion

2.1. Material Synthesis and Characterization

Considering eco-friendly solution-processable OSCs, three donor materials, namely P(F-FPy), P(F-FPy)(PM6 = 0.2), and PM6(FPy = 0.2), were synthesized by the Stille coupling polymerization from a combination of three monomers, including the F-substituted 2D benzodithiophene (FBDT), benzodithiophenedione (BDD), and FPy units (**Figure 1**a). The molar ratios of FBDT:BDD:FPy for P(F-FPy), P(F-FPy)(PM6 = 0.2), and PM6(FPy = 0.2) are 1.0:0:1.0, 1.0:0.2:0.8, and 1.0:0.8:0.2, respectively. The detailed synthetic procedures and structural characterization are presented in the Figures S1–S5 (Supporting Information). The asymmetric FPy unit with a non-covalent conformational dual-lock[31] on one side can provide a partial crack in the rigid polymer backbone, thereby improve the solubility in eco-friendly solvents under heating. Therefore, the solubilities of P(F-FPy), P(F-FPy)(PM6 = 0.2), and PM6(FPy = 0.2) in TL at 100°C were quantitatively measured to be 100 (which observed up to 100 mg), 78, and 32 mg mL^{-1}, respectively. The commercial sample PM6 could not be quantified because it did not fully dissolve in hot TL. The simple solubility tests of polymers are conducted and the results are summarized in Table S1 (Supporting Information). As the content of FPy unit increased in the polymer backbone, the polymers can be dissolved in the more desirable eco-friendly solvents. The number-average molecular weights (M_ns) of P(F-FPy), P(F-FPy)(PM6 = 0.2), and PM6(FPy = 0.2) were 26.30, 35.36, and 41.03 kDa, with correspond to polydispersity indices of 2.36, 2.52, and 2.26, respectively (Table S2, Supporting Information). All donor materials were thermally stable with decomposition temperatures of more than 350°C (Figure S6a, Supporting Information). In addition, no obvious thermal transition peak was observed for any of these materials during heating from

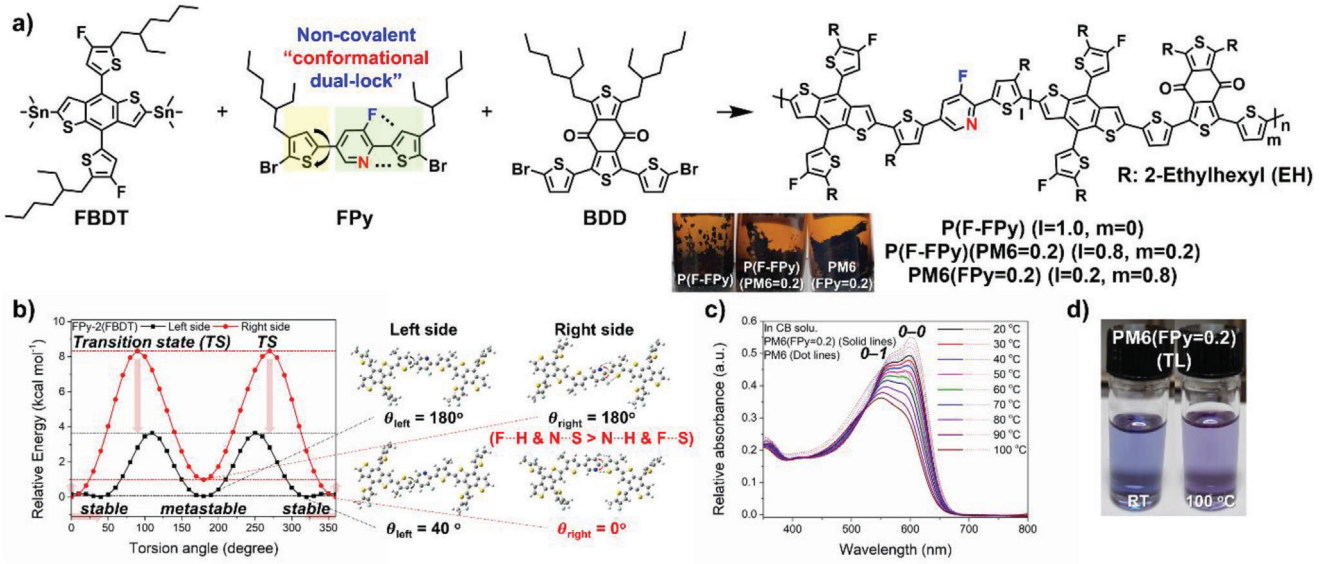

Figure 1. a) Synthetic routes and photographs of FPy-based polymer/terpolymers: P(F-FPy), P(F-FPy)(PM6 = 0.2), and PM6(FPy = 0.2). b) Relative potential energy scans as a function of the dihedral angles of the model compound FPy-2(FBDT) on left and right sides. (The red arrows represent the increasing steric hindrance). c) Temperature-dependent UV–vis absorption spectra of PM6(FPy = 0.2) and commercial PM6 in CB solutions. d) photographs of PM6(FPy = 0.2) in TL solutions at RT and 100°C, respectively.

room temperature to 300°C, indicating the absence of an inherent crystalline nature (Figure S6a, Supporting Information).

Density functional theory (DFT) calculations of the model compounds for donor materials were conducted to understand the influence of the FPy unit in the polymer backbone at two repeating units (Figures S7–S9, Supporting Information). All side chains of the model compounds were simplified with a methyl group. For the terpolymers, we used a model compound with 50% FPy in the backbone for computational ease.[32] As a reference substance, PM6 exhibits the smallest total dihedral angle (θ_{total}) of 8.03°, among the optimized geometries. In contrast, introducing 50% and 100% FPy, instead of BDD, into the backbone of PM6 achieved larger θ_{total}s of 58.72° and 14.09° for P(F-FPy), and P(F-FPy)(PM6 = 0.5), respectively. Therefore, FPy-based donor materials provide higher flexibility and solubility than PM6. The significantly higher dipole moments of P(F-FPy) and P(F-FPy)(PM6 = 0.5) are expected to increase the intramolecular charge transfer (ICT) and intermolecular interactions.[33,34] The energy levels of the frontier molecular orbitals, including the HOMO and lowest unoccupied molecular orbital (LUMO), are summarized in Table S3 (Supporting Information). The HOMO energy levels of all model compounds are similar with ≈5.0 eV and bandgap decreased in the order of P(F-FPy) < P(F-FPy)(PM6 = 0.5) < PM6, which can expect to increase the short-circuit current density (J_{sc}).[7] In addition, all model compounds exhibit continuous negative molecular electrostatic potential (ESP) surfaces, which are beneficial for charge extraction to the acceptor with relatively positive ESP surfaces.[35,36]

As shown in Figure 1b, the relative potential energy scan results of θ_{total} between flanked units for the model compound FPy-2(FBDT) has a considerably lower steric hindrance on the right side than on the left side (Table S4, Supporting Information).[37] The right side has a distinct stable conformation (0°) with a relatively deep energy, whereas the left side has two stable (40°) and metastable (180°) conformations with a similar energy. This difference is attributed to the non-covalent conformational dual-lock.[31] Therefore, the left-side structure can be freely adopted between stable and metastable conformations upon coating after heating. In contrast, the F···H and N···S bonds on the right side are stronger than the N···H and F···S bonds, which is highly likely to form a thermodynamically stable conformation. These results can significantly affect the aggregation behavior of the polymer. The tendency of the polymers to form aggregates or crystallize is an important feature for tuning the blend morphology, and can be studied by investigating the temperature-dependent aggregation (TDA) in the solution state.[38,39]

To better comprehend the aggregation properties of the FPy effect, temperature-dependent ultraviolet–visible (UV–vis) absorption profiles of PM6(FPy = 0.2) and PM6 in CB were obtained at 20–100°C (Figure 1c; Figure S10, Supporting Information). When the solution temperature was increased from 20 to 100°C, both spectra showed a gradual decrease in the ICT effect owing to the disaggregation of the polymers upon heating. In more detail, the intensity ratio of the 0–0 to 0–1 peaks (I_{0-0}/I_{0-1}) for PM6(FPy = 0.2) quantitatively shows a higher extent of disaggregation, compared to that of PM6 (Table S5, Supporting Information); thus, the I_{0-0}/I_{0-1} temperature with 1.0 or less is 50°C for PM6(FPy = 0.2) and 80°C for PM6. These results suggest that the polymeric chains of PM6(FPy = 0.2) disaggregated easily at relatively low temperatures, which is consistent with its significantly improved solubility in TL. In addition, higher pre-aggregation feature of PM6(FPy = 0.2) solutions is suggested to have a critical role in self-assembling a fiber-like network, which can result in the formation of an excellent interpenetrating morphology with the acceptor. Such aggregation behaviors of PM6(FPy = 0.2) were observed with a similar trend in TL (Figure S11 and Table S6, Supporting Information). In addition, the TL solution of PM6(FPy = 0.2) experienced an obvious color transition

Table 1. Photovoltaic performance of the optimized OSCs based on FPy-polymer/terpolymer:BTP-eC9.

Donor:BTP-eC9	Processing solvent	V_{oc} [V]	J_{sc} [mA cm^{-2}]	J_{cal} [mA cm^{-2}]	FF [%]	PCE_{max}/PCE_{ave}[a)] [%]
P(F-FPy)	TL (0.5% PN)	0.921	21.84	20.85	60.9	12.3/12.0 ± 0.24
P(F-FPy)(PM6 = 0.2)	TL (0.5% PN)	0.896	23.11	22.35	69.1	14.3/14.1 ± 0.23
PM6(FPy = 0.2)	CF (0.5% DIO)	0.841	26.42	26.25	76.5	17.0/16.7 ± 0.29
	TL (0.5% PN)	0.858	24.82	24.80	75.4	16.1/15.8 ± 0.30

[a)] Average PCE values calculated from 10 independent cells.

during heating (Figure 1d). Comprehensively, PM6(FPy = 0.2) can provide a pronounced TDA effect, which is an important feature for the effective control of blend morphologies.[20,38–40]

The detailed optical and electrochemical properties of the FPy-based polymer/terpolymers are presented in Figure S12 and Table S7 (Supporting Information). The optical bandgaps (E_g^{opt}s) of P(F-FPy), P(F-FPy)(PM6 = 0.2), and PM6(FPy = 0.2) are 2.10, 1.91, and 1.84 eV, respectively, which exhibits good complementary absorption with the BTP-eC9 acceptor.[7,32] Furthermore, all FPy-based donor materials have obvious 0–0 and 0–1 peaks in the film state despite their low crystalline structures in the solution state. The HOMO energy levels (E_{HOMO}s) of P(F-FPy), P(F-FPy)(PM6 = 0.2), and PM6(FPy = 0.2) were −5.71, −5.66, and −5.58 eV, respectively. These results are slightly different with the results of the DFT calculations, which can be attributed to the difference in the number of possible conformations derived from the asymmetric FPy unit introduced in each polymer backbone (Figure S13, Supporting Information).[13,37,41]

2.2. Eco-Friendly Solution-Processed OSCs

To investigate the eco-friendly solution-processed photovoltaic performance of FPy-based polymer/terpolymers, TL (0.5% 1-phenyl naphthalene, PN)-processed OSCs were fabricated and optimized with the conventional indium tin oxide (ITO)/ poly(3,4-ethylenedioxythiophene) polystyrene sulfonate (PEDOT:PSS)/donor:BTP-eC9/

Perylene-diimide (PDINN)/Ag structure. The detailed fabrication procedures of the OSCs are presented in the Supporting Information. The photovoltaic parameters of the optimized OSCs are summarized in **Table 1**. As shown in **Figure 2**a, BTP-eC9 was selected as the acceptor owing to its light-harvesting capability in the visible to near-infrared regions and well-matched energy-level alignment with the donor materials.[20,22,32] As shown in Figure 2b, as the HOMO levels of the donor materials decreased, V_{oc}s values of PM6(FPy = 0.2), P(F-FPy)(PM6 = 0.2), and P(F-FPy) gradually increased to 0.858, 0.896, and 0.921 V, respectively. In contrast, J_{sc}s and FFs gradually decreased from 24.82 to 21.84 mA cm^{-2} and 75.4 to 60.9%, respectively, with an opposite V_{oc} tendency. The PM6(FPy = 0.2):BTP-eC9-based OSC exhibited the highest PCE of 16.1% among the three eco-friendly solution-processed OSCs (PM6:BTP-eC9 showed a PCE of 15.2%; Table S8, Supporting Information). In addition, PM6(FPy = 0.2) reached the highest PCE of 17.0% using CF (0.5% 1,8-diiodooctane, DIO), which demonstrates the great potential of the polymer for high-efficiency OSCs. More importantly, PM6(FPy = 0.2)-based devices demonstrated an excellent batch-to-batch reproducibility in the M_n range of 20.09–41.03 kDa. All batches obtained with the polymerization time of over 36 h can provide an efficiency of ≈16% (Figure S14 and Table S9, Supporting Information).[8,13,31,32,42]

To investigate J_{sc}, the EQE curves of the OSCs were obtained, as shown in Figure 2c. All OSCs exhibit a broad photoresponse in the range of 300–900 nm, which indicate their effective light-harvesting capability. The calculated integrated current densities are consistent with those of the *J*–*V* curves with a mismatch of <5%. The CF-processed OSC of PM6(FPy = 0.2) exhibit significantly high EQEs of over 87% in the donor and acceptor main absorption regions.[20] Moreover, although the TL-processed OSC has lower EQE responses, it has superior *J*-aggregates and crystallinity in both the donor and acceptor. These results can be closely correlated to the molecular orientation and interpenetrating networks of the donor and acceptor.[18,20,22,32,38–40]

The molecular orientation behaviors of the representative FPy-based polymer and terpolymer, P(F-FPy), and PM6(FPy = 0.2), were investigated using 2D grazing incidence wide-angle X-ray scattering (2D-GIWAXS) measurements (Figure S15, Supporting Information).[8,17,32] The corresponding line-cut profiles in the out-of-plane (OOP; along q_z) and in-plane (IP; along q_{xy}) directions, and intensity-integrated azimuthal pole figure plots of the (100) scattering peaks were obtained (Figure S16, Supporting Information). The (100) and (010) distances ($d_{(100)}$ and $d_{(010)}$) were calculated using Bragg's law.[41] The integrated areas within the azimuthal angle in the range of 0–45° (A_z) and 45–90° (A_{xy}) are defined as the corresponding fractions of face-on and edge-on structures, respectively; thus, the face-on to edge-on ratio (A_{xy}/A_z) was calculated. Moreover, the (100) and (010) crystal coherence lengths ($CCL_{(100)}$ and $CCL_{(010)}$) in the OOP direction were calculated from the full width at half maximum (FWHM) value using the Scherrer equation.[41] The detailed 2D-GIWAXS parameters are summarized in Table S10 (Supporting Information).

For the neat films of P(F-FPy) and PM6(FPy = 0.2) processed with TL, both films simultaneously exhibit π–π stacking peaks at q_z = 1.655–1.672 Å^{-1} in the OOP and lamellar stacking peaks at q_{xy} = 0.276–0.284 Å^{-1} in the IP. The A_{xy}/A_z ratios of P(F-FPy) and PM6(FPy = 0.2) are 0.41 and 0.53, respectively, which suggest the edge-on dominance for both donor materials. Notably, PM6(FPy = 0.2) has a relatively close $d_{(010)}$ of 3.76 Å, and higher corresponding $CCL_{(010)}$ of 34.47 Å than that of P(F-FPy) (3.80 and 23.23Å, respectively). The shortened π–π stacking distance and large crystallite size can provide more efficient charge transport.[10,11,23,29,32]

When blended with the BTP-eC9 acceptor, the TL-processed P(F-FPy) and PM6(FPy = 0.2) films exhibit different molecular

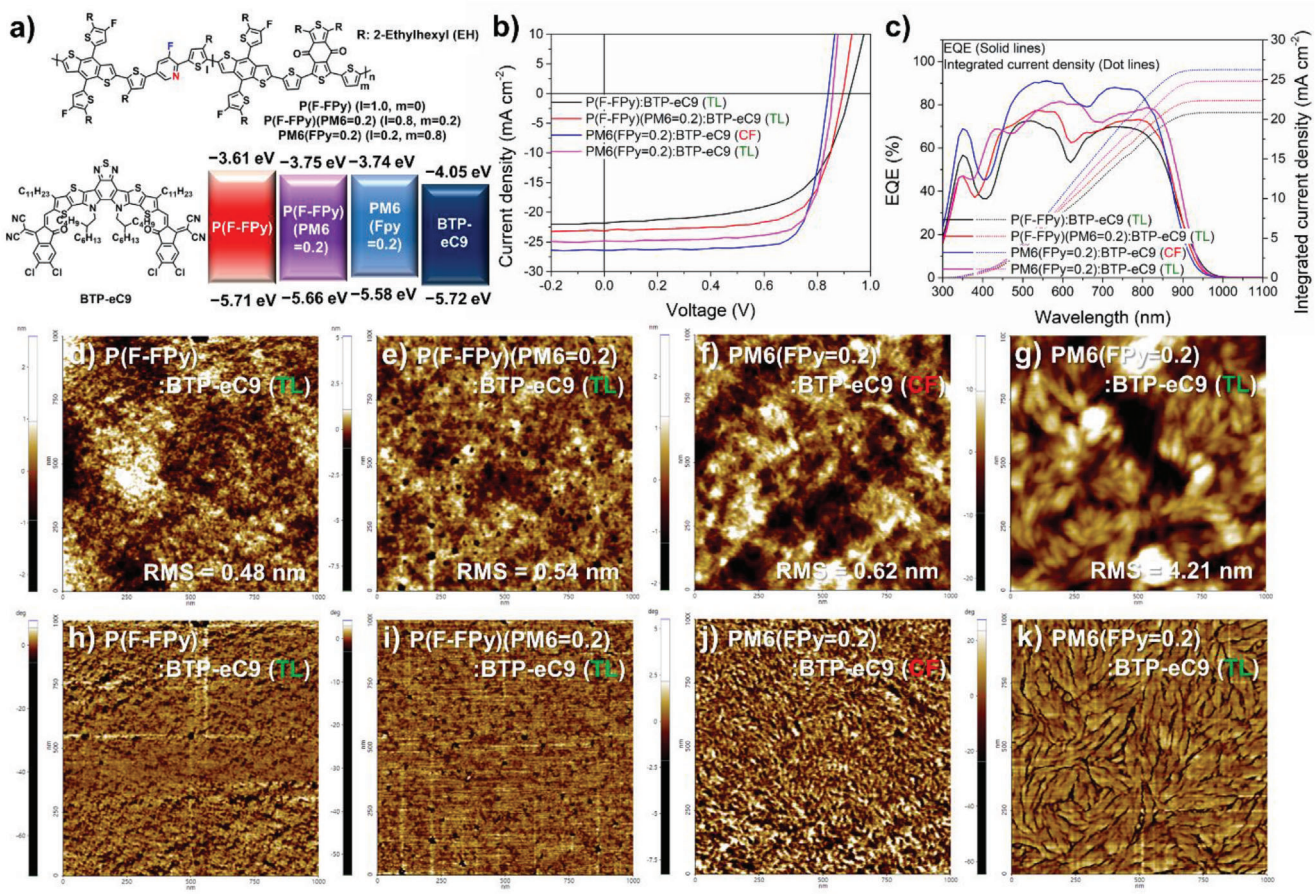

Figure 2. a) Molecular structures and energy level diagram of the FPy-based polymer/terpolymers and BTP-eC9. b) *J*–*V* and c) EQE curves of the optimized OSCs based on FPy-polymer/terpolymer:BTP-eC9. AFM d–g) height and h–k) phase images (1×1 μm) of the optimized FPy-polymer/terpolymer blend films.

packing behaviors. Although $d_{(100)}$ slightly increased, the P(F-FPy):BTP-eC9 film exhibited a dramatically reduced π–π stacking effect than that of the neat P(F-FPy) film. In addition, $CCL_{(100)}$, $CCL_{(010)}$, and A_{xy}/A_z ratio decreased. In contrast, PM6(FPy = 0.2):BTP-eC9 has the shortest $d_{(010)}$ of 3.64 Å and $d_{(100)}$ of 20.72 Å, which are beneficial for the charge transport in the vertical and horizontal directions.[11,32] However, $CCL_{(010)}$ is decreased by 15.51 Å, and $CCL_{(100)}$ increased by 68.33 Å. The CF-processed PM6(FPy = 0.2):BTP-eC9 film exhibited the same $d_{(100)}$ as the TL-processed blend film, and the largest $CCL_{(010)}$ and A_{xy}/A_z ratio of 40.29 and 0.97 Å, respectively. These results are consistent with the photovoltaic performance of OSCs.

To evaluate the charge transport properties of OSCs, we obtained their electron and hole mobilities (μ_e and μ_h) and balance ratio (μ_e/μ_h) using the space–charge-limited current (SCLC) characteristics of electron-only and hole-only devices (Figure S17 and Table S11, Supporting Information).[17,32,37,41] The details of the SCLC measurements are summarized in the Supporting Information. Briefly, the fabricated OSCs displayed a μ_e of 2.80×10^{-5}–9.65×10^{-4} and μ_h of 1.56×10^{-4}–7.24×10^{-4}, which gradually increased in the order of P(F-FPy):BTP-eC9 (TL) < P(F-FPy)(PM6 = 0.2):BTP-eC9 (TL) < PM6(FPy = 0.2):BTP-eC9 (TL) < PM6(FPy = 0.2):BTP-eC9 (CF). In particular, the μ_e/μ_h values are 0.18, 0.41, 1.52, and 1.33 for P(F-FPy):BTP-eC9 (TL), P(F-FPy)(PM6 = 0.2):BTP-eC9 (TL), PM6(FPy = 0.2):BTP-eC9 (TL), and PM6(FPy = 0.2):BTP-eC9 (CF), respectively, which are consistent with the photovoltaic results of the OSCs, especially the FF tendency.

To understand the distinguishing photovoltaic results of OSCs, we investigated the surface morphologies of the blend films through atomic force microscopy (AFM), as displayed in Figure 2d–k.[17,32,37,41] All blend films were prepared under the same conditions as the optimized devices. In the AFM height images in Figure 2d–g, the root–mean–square (RMS) roughness of P(F-FPy):BTP-eC9 (TL), P(F-FPy)(PM6 = 0.2):BTP-eC9 (TL), PM6(FPy = 0.2):BTP-eC9 (CF), and PM6(FPy = 0.2):BTP-eC9 (TL) films are 0.48, 0.54, 0.62, and 4.21 nm, respectively. As the amount of the FPy units in the polymer backbone decreases from 100% to 20%, the blend films gradually exhibit distinct surfaces and crystal grains along the RMS values. These results are observed in the corresponding AFM phase images in more detail (Figure 2h–k). In particular, the CF-processed PM6(FPy = 0.2):BTP-eC9 film shows bicontinuous interpenetrating networks with uniform nanofibril surfaces, which can boost the charge transport, resulting in high J_{sc} and FF values.[11,43,44] In contrast, the TL-processed PM6(FPy = 0.2):BTP-eC9 film has an oversized phase separation due to the high aggregation derived from its strong fibril networks between the donor and

Table 2. Photovoltaic performance of the optimized OSCs and ST-OSCs with different PM6(FPy = 0.2):BTP-eC9 ratios.

PM6(FPy = 0.2):BTP-eC9	V_{oc} [V]	J_{sc} [mA cm^{-2}]	J_{cal} [mA cm^{-2}]	FF [%]	PCE_{max}/PCE_{ave} [a)] [%]	AVT [%]	LUE [b)] [%]
1.0:1.0	0.858	24.82	24.80	75.4	16.1/15.8 ± 0.30	45.08[c)]	–
	0.831	20.03	19.16	73.1	12.2/11.8 ± 0.39	23.99	2.92
0.5:1.0	0.839	23.16	22.91	74.4	14.5/14.2 ± 0.31	56.29[c)]	–
	0.819	18.78	18.02	72.1	11.1/10.9 ± 0.33	32.58	3.61
0.25:1.0	0.827	20.68	19.47	72.2	12.4/12.2 ± 0.26	65.62[c)]	–
	0.831	14.99	14.23	71.7	8.9/8.6 ± 0.34	41.10	3.67
0.2:1.0	0.829	17.22	16.70	72.0	10.3/10.0 ± 0.24	68.72[c)]	–
	0.831	12.67	12.20	71.9	7.6/7.2 ± 0.39	42.44	3.31

[a)] Average PCE values calculated from 10 independent cells [b)] LUE = PCE × AVT [c)] AVT of the optimized polymer blend film.

acceptor.[28,29] Nevertheless, it is noteworthy that the device provided a high PCE of over 16% without the FF depression. These results support the SCLC results of the OSCs.

To further study the exciton dissociation and charge collection efficiencies of high-performance OSCs based on PM6(FPy = 0.2):BTP-eC9 processed by CF and TL, the plots of photocurrent density (J_{ph}) versus effective voltage (V_{eff}) were measured.[11,14,17–21,23,24,26,30,35,41,43] As shown in Figure S18a (Supporting Information), when V_{eff} >1.5 V, the J_{ph} values of two devices were saturated and, thus, all excitons were dissociated and all the generated charge carriers were collected. Therefore, the exciton dissociation (P_{diss}) and charge collection probabilities (P_{coll}) can be estimated from the J_{ph}/J_{sat} ratio at short-current condition and maximum power output. The P_{diss} values of CF and TL-processed devices were 99.4% and 99.3%, respectively, indicating that both devices enable the significant exciton dissociation. For P_{coll} values, CF-device with 99.1% showed a higher than that of value of TL-device (91.8%). These results are consistent with J_{sc} and FF values of the corresponding devices. The details of the relevant parameters are summarized in Table S12 (Supporting Information).

Successively, the photovoltaic parameters of CF and TL-processed devices were evaluated while changing the incident light intensity (P_{light}) (Figure S18b–d, Supporting Information).[11,14,17–21,23,24,26,30] According to the equation ($J_{sc} \propto P_{light}{}^{\alpha}$) of J_{sc}–P_{light} plots, α values were determined to be 0.998 and 0.993 for CF and TL-devices, respectively, which are very close to 1. Therefore, the bimolecular charge recombination can be negligible in both devices. The slopes (S) of V_{oc}–P_{light} plots for CF and TL-devices showed similar values with 1.07 and 1.08 $kT\,q^{-1}$, respectively (Here, k is the Boltzmann constant, T is the temperature, and q is the elementary charge). The relatively lower trap-assisted recombination was found for the CF-device likely due to the most balanced charge transport and is one of the origins of its high FF and overall device performance. These results suggest that the bimolecular recombination and trap-assisted recombination can be effectively reduced in both devices regardless of processing solvent and film morphology.

2.3. Eco-Friendly Solution-Processed ST-OSCs

Based on the eco-friendly and efficient photovoltaic performance and unique morphological features of PM6(FPy = 0.2), ST-OSCs were further investigated with the conventional structure of ITO/PEDOT:PSS/PM6(FPy = 0.2):BTP-eC9(x:y)/PDINN/Ag/WO_3. The Ag (10 nm)/WO_3 (30 nm) bilayer was introduced as the top electrode for the ST-OSCs, which can provide excellent transmittance and proper electrical resistance.[24,32,45] The detailed fabrication procedures of ST-OSCs are presented in the Supporting Information. To achieve valid photovoltaic performance and transmittance of ST-OSCs, the weight ratio of PM6(FPy = 0.2):BTP-eC9 was optimized to 1.0:1.0, 0.5:1.0, 0.25:1.0, and 0.2:1.0, respectively. The photovoltaic parameters of the OSCs and ST-OSCs with respect to the donor and acceptor weight ratios are summarized in **Table 2**.

It is well known that the photovoltaic performance of OSCs is strongly related with the donor and acceptor weight ratios. Therefore, the PCEs gradually decreased along the decrease of J_{sc}s from 16.1% to 10.3% when the donor and acceptor weight ratios were changed from 1.0:1.0 to 0.2:1.0 (**Figure 3**a,b), which are similar or slightly higher than the previously reported trend in the literature.[46] Surprisingly, despite the decreased donor content, the corresponding OSCs based on PM6(FPy = 0.2):BTP-eC9 with a ratio of up to 0.2:1.0 retained high FFs of over 72%. In addition, as shown in the transmittance spectra of the blend films for the optimized OSCs, the donor polymer PM6(FPy = 0.2) with ratios of 1.0, 0.5, 0.25, and 0.2 has the AVT of 45.08%, 56.29%, 65.62%, and 68.72%, respectively, for the active layers (Figure S19, Supporting Information). These results offer great opportunities for the fabrication of efficient ST-OSCs.

The highest PCE of 12.2% with an AVT of 23.99% was achieved with the PM6(FPy = 0.2):BTP-eC9 ratio of 1.0:1.0 With a decrease in the polymer ratio in the active layer, the PCEs decreased from 12.2% to 7.6%, and the AVTs increased from 23.99% to 42.44% (Figure 3a–c; Figure S20, Supporting Information). Compared to opaque OSCs, all ST-OSCs showed high tolerance to FF, which provide insights for future ST-OSC development. Considering the effectiveness of ST-OSCs, significantly high LUEs of 3.61% and 3.67% were achieved at the ratios of 0.5:1.0 and 0.25:1.0, respectively.

Importantly, the ST-OSC with a polymer ratio of 0.25:1.0 can be further highlighted through the Commission Internationale de l'Eclairage 1931 color space, color-rendering index (CRI), and correlated color temperature (CCT) (Figures S21 and S22 and Table S13, Supporting Information). As a result, in ST-OSC with a ratio of 0.25:1.0, the color coordinates were (0.290, 0.316). The transmittance at the most sensitive wavelength at 555 nm was

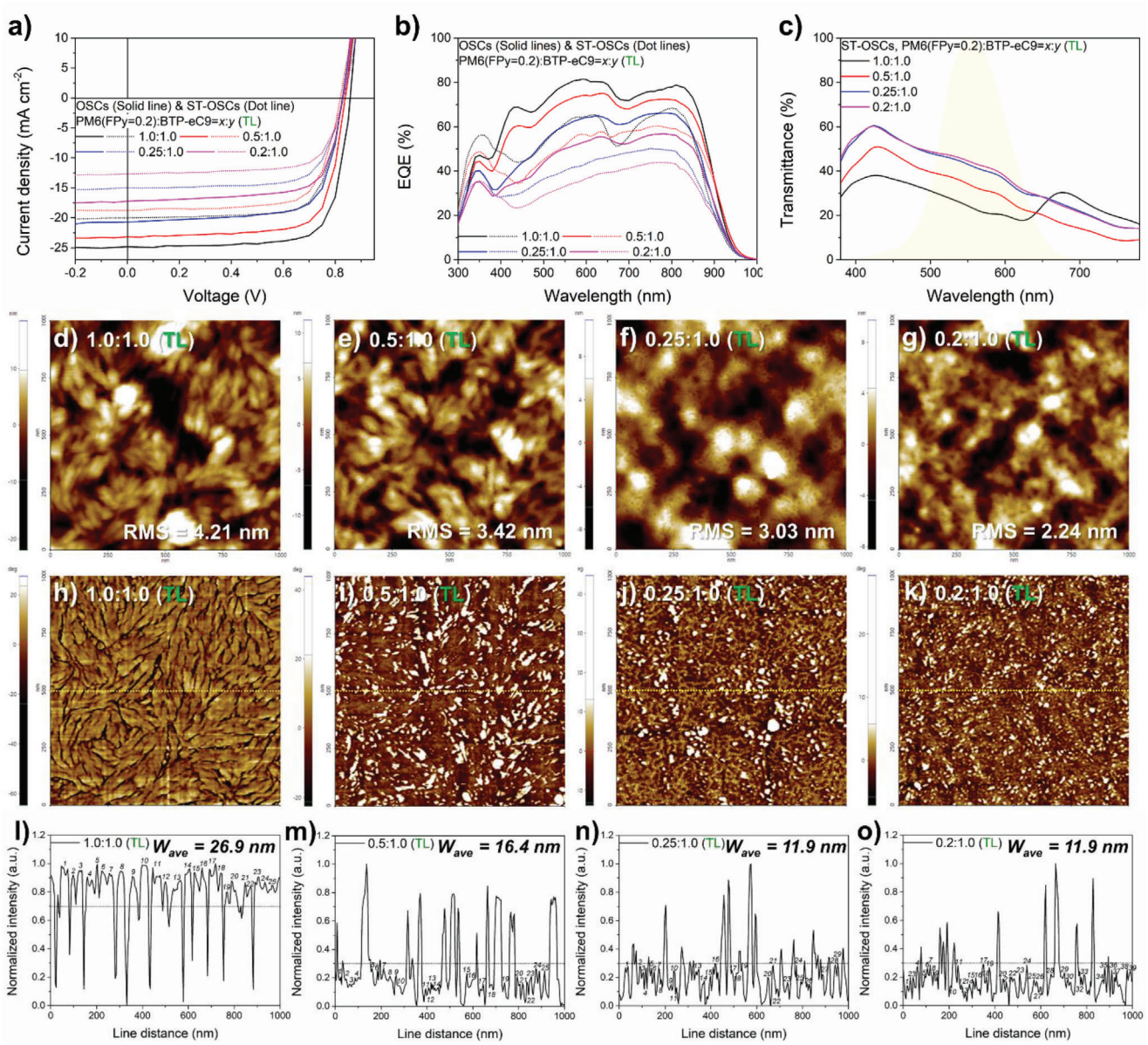

Figure 3. a) *J–V* and b) EQE curves of the optimized OSCs and ST-OSCs based on PM6(FPy = 0.2):BTP-eC9 processed with TL. c) Transmittance spectra of the optimized ST-OSCs (yellow region: photopic vision response). AFM d–g) height and h–k) phase images (1×1 µm) of the optimized PM6(FPy = 0.2)-based blend films, with respect to the donor-to-acceptor weight ratio. l–o) Line profiles to obtain the FWHM of the cross-sections using the AFM signals (yellow dot lines).

42.4% for human eyes. The CRI and CCT were 79.3 and 8104 K, respectively. These results demonstrate the superior potential for window applications of ST-OSCs with the ratio of 0.25:1.0 than those with the ratio of 0.5:1.0.[31,32,45,47]

To understand the contribution to the photovoltaic parameters of ST-OSCs, photoluminescence (PL) measurements were conducted in the neat and blend films with respect to the donor and acceptor weight ratio (Figure S23, Supporting Information).[13,17,33,37] The neat and blend films exhibit a pronounced PL emission peak in the range of 650–800 when excited at 612 nm. The excitation of the acceptor was not investigated owing to the technical issue of the PL machine. The PL quenching (PLQ) rates and energy-level offsets are summarized in Table S14 (Supporting Information). Briefly, the donor-to-blend PLQ rates ($PLQ_{D\rightarrow B}$) with the decreased donor weight ratio gradually decreased from 89.08% to 61.31%, which is consistent with the J_{sc} tendency of OSCs and ST-OSCs. These results correspond well with the decreased donor content, and LUMO and HOMO offsets between the donor and acceptor materials.

The results suggest that the photovoltaic performance of ST-OSCs is highly dependent on the FF values derived from the morphological characteristics, considering the decrease in the V_{oc} values with an imbalance in the donor and acceptor weight ratio.[46] As shown in Figure 3d–k, the decrease in the PM6(FPy = 0.2)

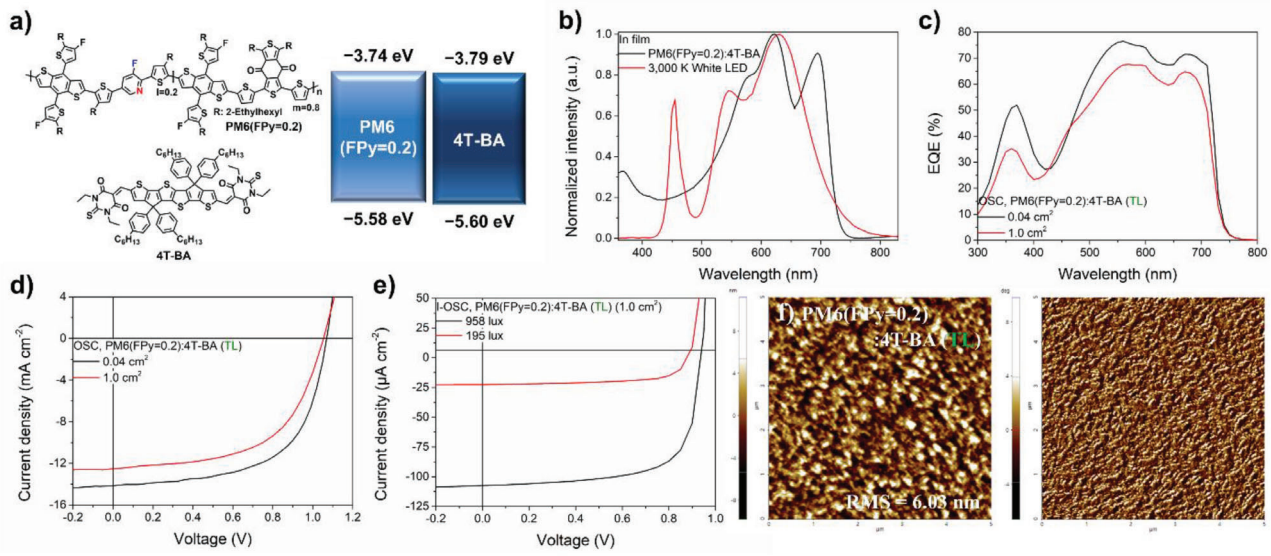

Figure 4. a) Molecular structures and energy level diagram of PM6(FPy = 0.2) and 4T-BA. b) UV–vis and emission spectrum of the PM6(FPy = 0.2):4T-BA film under a 3000 K white LED, respectively. c) EQE and d) *J–V* curves of the optimized OSCs based on PM6(FPy = 0.2):4T-BA with small and large areas (0.04 and 1.0 cm^2). e) *J–V* curves of the optimized large-area (1.0 cm^2) I-OSC based on PM6(FPy = 0.2):4T-BA under a 3000 K LED at 958 and 195 lux. f) AFM height and phase images (1×1 μm) of the optimized PM6(FPy = 0.2):4T-BA film.

content gradually decreased the highly aggregated morphology with the oversized fiber distribution, resulting in the reduced domain sizes in the blend surfaces. Moreover, the decrease in the PM6(FPy = 0.2) amount in the blends from 1.0 to 0.2 decreased the RMS values from 4.21 to 2.24 nm, which is opposite to the previously reported trend in the literature.[46] More importantly, the average fibril widths (W_{ave}), which provide high-speed channels for efficient exciton dissociation and charge transport,[9,48,49] in the corresponding phase images dramatically changed from 26.9 to 11.9 nm (Figure 3l–o). The results suggest that the fibril texture in the blends could be manipulated by controlling the PM6(FPy = 0.2) content.

As shown in Figure S24 and Table S15 (Supporting Information), the charge transport properties were investigated with respect to the donor-to-acceptor weight ratio. Substantially decreasing the amount of PM6(FPy = 0.2) did not affect μ_h and decreases μ_e: for the donor weight ratio gradually decreased, both μ_e and μ_h values showed 6.53×10^{-4} and 4.27×10^{-4} for 1.0:1.0, 4.54×10^{-4} and 4.42×10^{-4} for 0.5:1.0, 3.60×10^{-4} and 3.39×10^{-4} for 0.25:1.0, and 3.49×10^{-4} and 2.83×10^{-4} for 0.2:1.0, respectively. Notably, when the donor weight ratio decreased from 1.0 to 0.2, the drop rates of μ_hs are less with two times compared to those of μ_es. Encouragingly, the PM6(FPy = 0.2):BTP-eC9 films at ratios of 0.5:1.0 and 0.25:1.0 even achieved a high balance of μ_e/μ_h close to 1. Overall, the PM6(FPy = 0.2)-based blend system with a decreased donor weight ratio demonstrated that the well-distributed fibril networks ensured high FF values and resulted in outstanding ST-OSCs.[9,48,49]

2.4. Eco-Friendly Solution-Processed I-OSCs

We further examined the photovoltaic performance of eco-friendly I-OSCs by employing PM6(FPy = 0.2) under indoor lighting conditions (3000 K white LED). All devices for the I-OSCs were fabricated with an inverted structure of ITO/ZnO/PM6(FPy = 0.2):4T-BA/MoO_3/Ag. The detailed fabrication procedures of the I-OSCs are presented in the Supporting Information. Most the Internet of Things (IoTs) devices (sensors, bluetooth devices, smart electronic devices, etc.) usually work in an indoor environment and need enough high driving voltage (<1.0 V) to work well.[33] Hence, 4T-BA replacing of BTP-eC9 was adopted as the I-OSC acceptor to improve the opto-electrochemical properties and spectrum matching with PM6(FPy = 0.2) and LED (**Figure 4**a,b).[33] As shown in Figure S25 and Table S16 (Supporting Information), the 4T-BA film has an E_g^{opt} of 1.66 eV with a deep HOMO energy level of −5.60 eV and up-shifted LUMO energy level of −3.79 eV. Therefore, the PM6(FPy = 0.2):4T-BA blend system can cover the entire region from 450 to 750 nm, consistent with the LED spectrum,[14,15,35,50] which helps to minimize charge recombination and enhance V_{oc}.[7]

The photovoltaic performance of the OSCs based on PM6(FPy = 0.2):4T-BA with small and large areas of 0.04 and 1.0 cm^2 was first investigated. As shown in Figure 4c,d, with an area of 0.04 cm^2, a PCE of 9.1% was achieved with a V_{oc} of 1.07 V, J_{sc} of 14.15 mA cm^{-2}, and FF of 60.3%. It is noteworthy that the high V_{oc} is derived from the low E_{loss} of 0.61 eV. In OSCs with an area of 1.0 cm^2, a PCE of 7.5% is noted, along with decreased J_{sc} and FF values, owing to the low tolerance to the thickness and uniformity in the large-area device.[15,35,51] Nevertheless, the EQE curves of both OSCs show a good photoresponse spectrum from 300 to 750 nm, which meets the spectral requirement for indoor applications. Considering the photoactive combination with a V_{oc} of over 1.05 V, the high J_{sc}s of OSCs are well described by the PL results (Figure S26 and Table S17, Supporting Information). The low acceptor-to-blend PLQ rate ($PLQ_{A\rightarrow B}$) of 75.15% is might be attributed to the morphology related *D/A* interfaces.

Table 3. Photovoltaic performance of the optimized I-OSCs based on PM6(FPy = 0.2):4T-BA with respect to the light intensity.

Active area	Light intensity (source) [lux]	P_{in} [μW cm^{-2}]	V_{oc} [V]	J_{sc} [μA cm^{-2}]	J_{cal} [μA cm^{-2}]	FF [%]	P_{out} [μW cm^{-2}]	PCE_{max} /PCE_{ave}[a)] [%]
0.04 cm^2	(AM 1.5G)	100000	1.07	14153	13832	60.3	9138	9.1/8.9 ± 0.21
			1.05	12517	12060	56.9	7510	7.5/7.2 ± 0.29
1.0 cm^2	958(3000 K LED)	337.07	0.936	107.51	106.80	69.1	69.53	20.6/20.3 ± 0.34
	195(3000 K LED)	68.63	0.876	22.60	21.78	66.3	13.13	19.1/18.7 ± 0.39

[a)] Average PCE values calculated from 10 independent cells.

These results are consistent with the SCLC results (Figure S27 and Table S18, Supporting Information).

The photovoltaic performance of the I-OSCs was investigated under a 3000 K white LED at 958 and 195 lux, which represent the illumination conditions for typical indoor environments, such as supermarkets, offices, and living rooms.[14,15,35,50] The intensity of the indoor light was measured with a spectrometer for high reliability.[51–53] In addition, the indoor photovoltaic performance was evaluated in the large-area (1.0 cm^2) OSC, considering the measurement errors derived from the non-parallelism of indoor light.[15,35,51,52] For the 3000 K LED lamp, the input power density of the emission spectrum for each illuminance was accurately obtained by direct measurement using a calibrated spectrometer in a dark room (Figures S28 and S29, Supporting Information).[51–53]

Figure 4e and **Table 3** show the *J*–*V* curves and photovoltaic parameters of the large-area (1.0 cm^2) I-OSC under two illumination conditions. Based on the EQE curve of the OSC (Figure 4c) and photon flux spectrum (Figure S30, Supporting Information), the integrated current densities, which are consistent with the J_{sc} values from the *J*–*V* measurements, were calculated, thereby confirming the reliability of the I-OSCs. For the PM6(FPy = 0.2):4T-BA system, the output power densities of the I-OSC were 69.53 and 13.13 μW cm^{-2} with PCEs of 20.6% and 19.1% under 958 and 195 lux, respectively. These results suggest that the PM6(FPy = 0.2)-based I-OSCs can provide power in real time for IoT sensors/mini-electronics with low power consumption.[27,50] In addition, it should be noted that the PCE values can be further improved using a 2700 K LED with enhanced emission in the long-wavelength region.[15,27,35,51]

To understand the photovoltaic performance of I-OSCs, the charge generation, transportation, and recombination dynamics of the PM6(FPy = 0.2):4T-BA device (1.0 cm^2) were examined by plotting the J_{ph}–V_{eff} and the J_{sc}/V_{oc}/FF–P_{light} (Figure S31, Supporting Information).[11,14,17–21,23,24,26,30,35,41,43] As shown in Figure S30a (Supporting Information), the P_{diss} value was calculated to be 96.6%. This value is similar compared to that of high-performance active combinations, which indicates efficient exciton dissociation and accounts in high J_{sc} of the device.[11,14,17–21,23,24,26] In contrast, the P_{coll} value showed a lower value of 77.4% which might be caused a relatively low FF in the device. The details of the relevant parameters are summarized in Table S19 (Supporting Information).

Next, to analyze closely the charge recombination processes of the device at AM 1.5G and 3000 K White LED environments, the photovoltaic parameters were evaluated with respect to the different P_{light} (Figure S31b–d, Supporting Information). The α values estimated from J_{sc}–P_{light} plots were determined to be 0.99 and 0.98 for high-light intensities (>10 mW cm^{-2}) and low-light intensities (<10 mW cm^{-2}), respectively, which means that the bimolecular charge recombination behaviors under low-light conditions are relatively high compared to those of high-light conditions. The *S* values estimated from V_{oc}–P_{light} plots for high and low-intensities were determined to be 1.07 and 1.06 $kT\ q^{-1}$, respectively. The relatively lower *S* value suggested the trap-assisted charge recombination of the device can be suppressed in low-light environment. Finally, the FF–P_{light} plots of the device follow a bell-shaped curve under the whole light intensities.[49] Comprehensively, these findings demonstrate that the PM6(FPy = 0.2):4T-BA-based device has negligible charge recombination behaviors in the both light environments.

Finally, the morphological properties of the PM6(FPy = 0.2):4T-BA film were analyzed. This blend film exhibited a fibrillar feature associated with the self-aggregation of the polymer with a large RMS of 6.03 nm, as displayed in Figure 4f, which hinders the efficient charge transport, results in a low FF.[30,39] However, in the corresponding phase image, bi-continuous networks are observed with distinguishable phase separation, which induced efficient charge separation and resulted in a relatively high J_{sc}.[9,46,49] These results are consistent with the aforementioned charge transport properties obtained by the PL and SCLC measurements.

2.5. Long-Term Stability of OSCs/ST-OSCs/I-OSC

Eco-friendly solution-processed devices have not been extensively studied in terms of their stability. In particular, the long-term device operation of eco-friendly solution-processed photoactive material and solvent/additive is still unclear.[12] Herein, to examine the long-term stability of OSCs/ST-OSCs/I-OSC with various blend films, encapsulated devices based on PM6(FPy = 0.2) were evaluated according to the shelf protocol of ISOS-D-1.[12,37,54,55] For the OSCs with the FPy-based donor and BTP-eC9, the corresponding PCEs continuously decreased for ≈500 h, as shown in **Figure 5**a. The degradation rates of the PCEs aggregate increased in order of P(F-FPy)(PM6 = 0.2):BTP-eC9 (TL) < P(F-FPy):BTP-eC9 (TL) < PM6(FPy = 0.2):BTP-eC9 (CF) < PM6(FPy = 0.2):BTP-eC9 (TL). These results can be closely correlated with the aggregation and fibril network of the polymer blends.[12,37,39,42,54,55]

As shown in Figure S32 (Supporting Information), V_{oc}s remained almost unchanged, whereas the J_{sc}s and FFs decreased significantly after ≈500 h. In detail, the PCE drops are similar to the FF tendency, and the drop rates of the PCEs were determined along with the J_{sc}s trend. Notably, the drop rates of J_{sc}s decreased as the fibril networks are increased. In general, the presence of

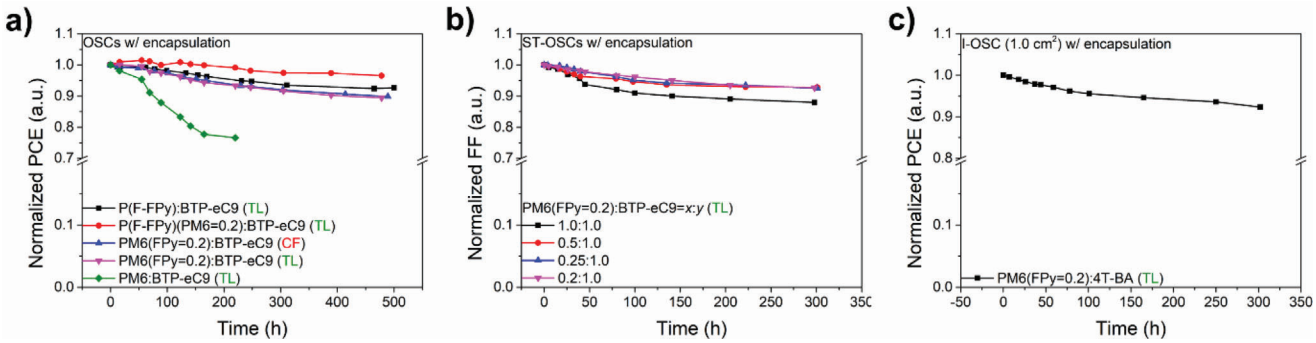

Figure 5. Long-term stability test curves of a) OSCs, b) ST-OSCs, and c) 1.0 cm^2 I-OSC with encapsulation according to the ISOS-D-1: a) P(F-FPy):BTP-eC9 (TL), P(F-FPy)(PM6 = 0.2):BTP-eC9 (TL), PM6(FPy = 0.2):BTP-eC9 (CF), PM6(FPy = 0.2):BTP-eC9 (TL), and PM6:BTP-eC9 (TL). b) PM6(FPy = 0.2):BTP-eC9 (*x*:*y*, 1.0:1.0, 0.5:1.0, 0.25:1.0, and 0.2:1.0; TL). c) PM6(FPy = 0.2):4T-BA (TL).

the residual additives can affect long-term stability because they are difficult to completely remove owing to their high boiling points.[12,30] Therefore, the DIO additive with high polarity and a linear aliphatic chain may cause morphological migration, compared with a relatively non-polar PN additives enabling the π–π stacking between the donor and acceptor.

As shown in Figure 5b, for the ST-OSCs with different PM6(FPy = 0.2):BTP-eC9 ratios, the corresponding PCEs continuously decreased for ≈300 h. The burn-in loss of ST-OSCs was alleviated as the donor content decreased in the polymer blend. In addition, the long-term stability of ST-OSCs is consistent with the morphological changes, such as RMS and fibril structure. The results suggest that the efficiency, transparency, and stability of the ST-OSCs can be improved by manipulating the PM6(FPy = 0.2) content in the polymer blend. The detailed photovoltaic parameter trends are shown in Figure S33 (Supporting Information). Finally, the long-term stability of the I-OSC based on PM6(FPy = 0.2):4T-BA was investigated under a 3000 K LED at 958 lux (Figure 5c; Figure S34, Supporting Information). As a result, excellent stability with the initial PCE maintained at 92.4% for 300 h was exhibited. Therefore, eco-friendly solution-processed OSCs/ST-OSCs/I-OSCs based on PM6(FPy = 0.2) was successfully demonstrated to provide an effective approach for the improvement of device performance and stability.

3. Conclusion

In summary, three FPy-based donor materials (P(F-FPy), P(F-FPy)(PM6 = 0.2), and PM6(FPy = 0.2)) were designed and synthesized to achieve high solubility in eco-friendly solvents, such as TL. The asymmetric FPy unit endowed unique features of the aggregation and fibril networks in the polymer blend backbone owing to its non-covalent conformational dual-lock on one side. Among FPy-based donor materials, PM6(FPy = 0.2) has great potential for eco-friendly solution-processed versatile OSCs. In particular, TL-processed OSCs/ST-OSCs/I-OSCs based on PM6(FPy = 0.2) exhibited high performance with 16.1% PCE in OSC, 3.67% LUE in ST-OSC (at 25% donor content), and 20.6% PCE in I-OSC (under the 3000 K LED at 958 lux). Furthermore, the efficiency and stability for all devices were closely correlated to the morphological properties of the donor and acceptor blends through long-term stability tests, according to the shelf protocol of ISOS-D-1. Therefore, this study opens a new perspective for designing various classes of polymer blends as a feasible and promising strategy for eco-friendly, efficient, and stable OSCs/ST-OSCs/I-OSCs.

Supporting Information

Supporting Information is available from the Wiley Online Library or from the author.

Acknowledgements

This work was supported by the Konkuk University in 2018.

Conflict of Interest

The authors declare no conflict of interest.

Data Availability Statement

The data that support the findings of this study are available from the corresponding author upon reasonable request.

Keywords

3-fluoropyridine, eco-friendly, indoor organic solar cells, semi-transparent organic solar cells, solubility

Received: March 1, 2023
Revised: May 1, 2023
Published online:

[1] Y. Hu, J. Wang, C. Yan, P. Cheng, *Nat. Rev. Mater.* **2022**, *7*, 836.
[2] G. P. Kini, S. J. Jeon, D. K. Moon, *Adv. Funct. Mater.* **2021**, *31*, 2007931.
[3] M. Riede, D. Spoltore, K. Leo, *Adv. Energy Mater.* **2021**, *11*, 2002653.
[4] M. Moser, A. Wadsworth, N. Gasparini, I. McCulloch, *Adv. Energy Mater.* **2021**, *11*, 2100056.
[5] R. Xue, J. Zhang, Y. Li, Y. Li, *Small* **2018**, *14*, 1801793.

[6] J. Yuan, Y. Zhang, L. Zhou, G. Zhang, H. L. Yip, T. K. Lau, X. Lu, C. Zhu, H. Peng, P. A. Johnson, M. Leclerc, Y. Cao, J. Ulanski, Y. Li, Y. Zou, *Joule* **2019**, *3*, 1140.
[7] S. Li, C. Z. Li, M. Shi, H. Chen, *ACS Energy Lett.* **2020**, *5*, 1554.
[8] Y. W. Han, S. J. Jeon, H. S. Lee, H. Park, K. S. Kim, H. W. Lee, D. K. Moon, *Adv. Energy Mater.* **2019**, *9*, 1902065.
[9] L. Zhu, M. Zhang, J. Xu, C. Li, J. Yan, G. Zhou, W. Zhong, T. Hao, J. Song, X. Xue, Z. Zhou, R. Zeng, H. Zhu, C. C. Chen, R. C. I. MacKenzie, Y. Zou, J. Nelson, Y. Zhang, Y. Sun, F. Liu, *Nat. Mater.* **2022**, *21*, 656.
[10] R. Ma, C. Yan, J. Yu, T. Liu, H. Liu, Y. Li, J. Chen, Z. Luo, B. Tang, X. Lu, G. Li, H. Yan, *ACS Energy Lett.* **2022**, *7*, 2547.
[11] Y. Wei, Z. Chen, G. Lu, N. Yu, C. Li, J. Gao, X. Gu, X. Hao, G. Lu, Z. Tang, J. Zhang, Z. Wei, X. Zhang, H. Huang, *Adv. Mater.* **2022**, *34*, 2204718.
[12] S. Lee, D. Jeong, C. Kim, C. Lee, H. Kang, H. Y. Woo, B. J. Kim, *ACS Nano* **2020**, *14*, 14493.
[13] X. Yuan, Y. Zhao, T. Zhan, J. Oh, J. Zhou, J. Li, X. Wang, Z. Wang, S. Pang, P. Cai, C. Yang, Z. He, Z. Xie, C. Duan, F. Huang, Y. Cao, *Energy Environ. Sci.* **2021**, *14*, 5530.
[14] L. K. Ma, Y. Chen, P. C. Y. Chow, G. Zhang, J. Huang, C. Ma, J. Zhang, H. Yin, A. M. H. Hong Cheung, K. S. Wong, S. K. So, H. Yan, *Joule* **2020**, *4*, 1486.
[15] Y. Cui, Y. Wang, J. Bergqvist, H. Yao, Y. Xu, B. Gao, C. Yang, S. Zhang, O. Inganäs, F. Gao, J. Hou, *Nat. Energy* **2019**, *4*, 768.
[16] L. Ye, Y. Xiong, Z. Chen, Q. Zhang, Z. Fei, R. Henry, M. Heeney, B. T. O'Connor, W. You, H. Ade, *Adv. Mater.* **2019**, *31*, 1808153.
[17] S. J. Jeon, Y. W. Han, D. K. Moon, *Small* **2019**, *15*, 1902598.
[18] Y. Luo, X. Wang, M. Zhang, X. Sun, A. Saparbaev, S. Lei, J. Zhang, B. Xiao, C. Yang, Z. Liu, R. Yang, *Sol. RRL* **2022**, *6*, 2200679.
[19] S. Jung, Y. Cho, Y. Ji, J. Oh, G. Park, W. Kim, S. Jeong, S. M. Lee, S. Chen, Y. Zhang, C. Yang, *Nano Energy* **2023**, *106*, 108059.
[20] C. Lim, S. Lee, D. Han, C. Lee, B. J. Kim, *Macromolecules* **2022**, *55*, 10395.
[21] H. Lu, H. Wang, G. Ran, S. Li, J. Zhang, Y. Liu, W. Zhang, X. Xu, Z. Bo, *Adv. Funct. Mater.* **2022**, *32*, 2203193.
[22] J. W. Lee, C. Lim, S. W. Lee, Y. Jeon, S. Lee, T. S. Kim, J. Y. Lee, B. J. Kim, *Adv. Energy Mater.* **2022**, *12*, 2270197.
[23] S. Rasool, J. W. Kim, H. W. Cho, Y. J. Kim, D. C. Lee, C. B. Park, W. Lee, O. H. Kwon, S. Cho, J. Y. Kim, *Adv. Energy Mater.* **2022**, *13*, 2203452.
[24] S. Guan, Y. Li, K. Yan, W. Fu, L. Zuo, H. Chen, *Adv. Mater.* **2022**, *34*, 2205844.
[25] D. Wang, H. Liu, Y. Li, G. Zhou, L. Zhan, H. Zhu, X. Lu, H. Chen, C. Z. Li, *Joule* **2021**, *5*, 945.
[26] J. Y. Fan, Z. X. Liu, J. Rao, K. Yan, Z. Chen, Y. Ran, B. Yan, J. Yao, G. Lu, H. Zhu, C. Z. Li, H. Chen, *Adv. Mater.* **2022**, *34*, 2110569.
[27] Q. Wu, Y. Yu, X. Xia, Y. Gao, T. Wang, R. Sun, J. Guo, S. Wang, G. Xie, X. Lu, E. Zhou, J. Min, *Joule* **2022**, *6*, 2138.
[28] L. Zhu, M. Zhang, W. Zhong, S. Leng, G. Zhou, Y. Zou, X. Su, H. Ding, P. Gu, F. Liu, Y. Zhang, *Energy Environ. Sci.* **2021**, *14*, 4341.
[29] X. Xu, L. Yu, H. Yan, R. Li, Q. Peng, *Energy Environ. Sci.* **2020**, *13*, 4381.
[30] C. McDowell, M. Abdelsamie, M. F. Toney, G. C. Bazan, *Adv. Mater.* **2018**, *30*, 1707114.
[31] D. Xie, Y. Zhang, X. Yuan, Y. Li, F. Huang, Y. Cao, C. Duan, *Adv. Funct. Mater.* **2022**, *33*, 2212601.
[32] S. J. Jeon, N. G. Yang, Y. H. Kim, J. H. Yun, D. K. Moon, *ACS Appl Mater Interfaces* **2022**, *14*, 38031.
[33] X. Liao, Y. Cui, X. Shi, Z. Yao, H. Zhao, Y. An, P. Zhu, Y. Guo, X. Fei, L. Zuo, K. Gao, F. Lin, Q. Xie, L. Chen, W. Ma, Y. Chen, A. K.-Y. Jen, *Mater. Chem. Front.* **2020**, *4*, 1507.
[34] G. P. Kini, S. J. Jeon, D. K. Moon, *Adv. Mater.* **2020**, *32*, 1906175.
[35] P. Bi, C. An, T. Zhang, Z. Chen, Y. Xu, Y. Cui, J. Wang, J. Li, Y. Wang, J. Ren, X. Hao, S. Zhang, J. Hou, *J. Mater. Chem.* **2023**, *11*, 983.
[36] L. Ma, H. Yao, J. Wang, Y. Xu, M. Gao, Y. Zu, Y. Cui, S. Zhang, L. Ye, J. Hou, *Angew. Chem., Int. Ed.* **2021**, *60*, 15988.
[37] S. J. Jeon, J. E. Yu, Y. W. Han, I. S. Suh, D. K. Moon, *J. Ind. Eng. Chem.* **2019**, *71*, 137.
[38] C. An, J. Hou, *Acc. Mater. Res.* **2022**, *3*, 540.
[39] M. Gao, W. Wang, J. Hou, L. Ye, *Aggregate* **2021**, *2*, e46.
[40] H. Bin, J. Li, A. Caiazzo, M. M. Wienk, Y. Li, R. A. J. Janssen, *ChemSusChem* **2023**, *16*, 202300006.
[41] S. J. Jeon, Y. W. Han, D. K. Moon, *ACS Appl. Mater. Interfaces* **2019**, *11*, 9239.
[42] K. Weng, L. Ye, L. Zhu, J. Xu, J. Zhou, X. Feng, G. Lu, S. Tan, F. Liu, Y. Sun, *Nat. Commun.* **2020**, *11*, 2855.
[43] L. Zhou, L. Meng, J. Zhang, S. Qin, J. Zhang, X. Li, J. Li, Z. Wei, Y. Li, *Adv. Sci.* **2022**, *9*, 2203513.
[44] C. Li, J. Zhou, J. Song, J. Xu, H. Zhang, X. Zhang, J. Guo, L. Zhu, D. Wei, G. Han, J. Min, Y. Zhang, Z. Xie, Y. Yi, H. Yan, F. Gao, F. Liu, Y. Sun, *Nat. Energy* **2021**, *6*, 605.
[45] K. Chen, N. Fan, H. Huang, X. Jiang, S. Qin, W. Xiao, Q. Zheng, Y. Zhang, X. Duan, Z. Qin, Y. Liu, J. Zeng, Y. Wei, X. Song, *Adv. Funct. Mater.* **2022**, *32*, 2204692.
[46] Y. Xie, Y. Cai, L. Zhu, R. Xia, L. Ye, X. Feng, H. L. Yip, F. Liu, G. Lu, S. Tan, Y. Sun, *Adv. Funct. Mater.* **2020**, *30*, 2002181.
[47] C. J. Traverse, R. Pandey, M. C. Barr, R. R. Lunt, *Nat. Energy* **2017**, *2*, 849.
[48] Y. Li, Y. Cai, Y. Xie, J. Song, H. Wu, Z. Tang, J. Zhang, F. Huang, Y. Sun, *Energy Environ. Sci.* **2021**, *14*, 5009.
[49] M. Zhang, L. Zhu, T. Hao, G. Zhou, C. Qiu, Z. Zhao, N. Hartmann, B. Xiao, Y. Zou, W. Feng, H. Zhu, M. Zhang, Y. Zhang, Y. Li, T. P. Russell, F. Liu, *Adv. Mater.* **2021**, *33*, 2007177.
[50] L. Xie, W. Song, J. Ge, B. Tang, X. Zhang, T. Wu, Z. Ge, *Nano Energy* **2021**, *82*, 105770.
[51] Y. Cui, H. Yao, T. Zhang, L. Hong, B. Gao, K. Xian, J. Qin, J. Hou, *Adv. Mater.* **2019**, *31*, 1808356.
[52] Y. Cui, L. Hong, T. Zhang, H. Meng, H. Yan, F. Gao, J. Hou, *Joule* **2021**, *5*, 1016.
[53] K. D. Rosenthal, M. P. Hughes, B. R. Luginbuhl, N. A. Ran, A. Karki, S. J. Ko, H. Hu, M. Wang, H. Ade, T. Q. Nguyen, *Adv. Energy Mater.* **2019**, *9*, 1901077.
[54] S. J. Jeon, Y. W. Han, Y. H. Kim, D. K. Moon, *Sol. RRL* **2020**, *4*, 2000074.
[55] S. J. Jeon, Y. W. Han, D. K. Moon, *Sol. RRL* **2019**, *3*, 1900094.